HHS Public Access

Author manuscript

*Sci Transl Med*. Author manuscript; available in PMC 2015 June 10.

Published in final edited form as:

*Sci Transl Med*. 2014 December 10; 6(266): 266ra170. doi:10.1126/scitranslmed.3010189.

# Visnagin protects against doxorubicin-induced cardiomyopathy through modulation of mitochondrial malate dehydrogenase

**Yan Liu**[1,2,†], **Aarti Asnani**[1,2,†], **Lin Zou**[3], **Victoria L. Bentley**[4], **Min Yu**[5], **You Wang**[1,2], **Graham Dellaire**[4], **Kumar S. Sarkar**[1,2], **Matthew Dai**[1], **Howard H. Chen**[1,6], **David E. Sosnovik**[1,6], **Jordan T. Shin**[1], **Daniel A. Haber**[5,7], **Jason N. Berman**[4], **Wei Chao**[3], and **Randall T. Peterson**[1,2,*]

[1]Cardiovascular Research Center, Massachusetts General Hospital and Harvard Medical School, Charlestown, Massachusetts 02129

[2]Broad Institute, Cambridge, Massachusetts 02142

[3]Department of Anesthesia, Critical Care and Pain Medicine, Massachusetts General Hospital and Harvard Medical School, Charlestown, Massachusetts 02129

[4]Department of Pathology and Biochemistry & Molecular Biology, Dalhousie University, Halifax, Nova Scotia, B3H4R2, Canada

[5]Massachusetts General Hospital Cancer Center and Harvard Medical School, Charlestown, Massachusetts 02129

[6]Martinos Center for Biomedical Imaging, Massachusetts General Hospital and Harvard Medical School, Charlestown, Massachusetts 02129

[7]Howard Hughes Medical Institute

## Abstract

Doxorubicin is a highly effective anti-cancer chemotherapy agent, but its usage is limited by its cardiotoxicity. To develop a drug that prevents the cardiac toxicity of doxorubicin while preserving its anti-tumor potency, we established a doxorubicin-induced cardiomyopathy model in zebrafish that recapitulated the cardiomyocyte apoptosis and contractility decline observed in patients. Using this model, we screened 3000 compounds and discovered that visnagin (VIS) and diphenylurea (DPU) rescue cardiac performance and circulatory defects caused by doxorubicin treatment in zebrafish. VIS and DPU reduced doxorubicin-induced apoptosis in cultured cardiomyocytes and in vivo in zebrafish and mouse hearts. Furthermore, VIS treatment improved

*Corresponding author: rtpeterson@mgh.harvard.edu.
†These authors contributed equally.

**Author Contributions:** Y.L., A.A., K.S.S. and R.T.P. conceived and carried out the screen. Y.W. synthesized the bergapten-coupled Affigel beads. M.D. and J.T.S. analyzed cardiac function in zebrafish. L.Z. and W.C. performed mouse echocardiography. H.H.C. and D.E.S. performed mouse cardiac imaging. V.L.B., G.D., and J.N.B. designed and carried out the zebrafish xenograft studies. M.Y. and D.A.H. designed and carried out the mouse xenograft studies. All authors contributed to the interpretation of data and writing of the paper.

**Competing Interests:** YL and RTP have applied for patents on the compounds described in this manuscript (PCT/US13/041334, Cardioprotective compounds, their use with chemotherapy, and methods for identifying them). The other authors declare that they have no other competing interests.

**Data and Material Availability**: Data and replicable biological materials available upon request.

cardiac contractility in doxorubicin-treated mice. Importantly, VIS and DPU caused no reduction in the chemotherapeutic efficacy of doxorubicin in several cultured tumor lines or in zebrafish and mouse xenograft models. Using affinity chromatography, we discovered that VIS binds to mitochondrial malate dehydrogenase (MDH2), one of the key enzymes in the tricarboxylic acid cycle. As with VIS, treatment with the MDH2 inhibitors mebendazole, thyroxine, and iodine prevented doxorubicin cardiotoxicity, as did treatment with malate itself, suggesting that modulation of MDH2 activity is responsible for VIS's cardioprotective effects. Taken together, this study identified VIS and DPU as potent cardioprotective compounds and implicates MDH2 as a previously undescribed, druggable target for doxorubicin-induced cardiomyopathy.

## Introduction

Doxorubicin is a potent chemotherapy drug widely used against a broad range of cancers including solid tumors and leukemia. Like other members of the anthracycline class, its usage is greatly limited by the risk of severe cardiotoxicity, and cumulative dosages above 300mg/m$^2$ exponentially increase the risk of heart failure (1). Even at lower doses, some patients inevitably develop heart disease many years after therapy (2). Therefore, adjuvant therapies that protect the heart but do not interfere with tumor treatment are needed. Such drugs could benefit cancer patients by preventing cardiomyopathy and by permitting the use of more effective anthracycline dosages.

The underlying mechanisms of anthracycline cardiotoxicity have not been fully elucidated. A plethora of proapoptotic effects such as DNA damage, lipid peroxidation, reactive oxygen species (ROS) overproduction, calcium mishandling, ATP depletion, contractile protein degradation and transcription misregulation have all been associated with anthracycline treatment (3, 4). Several of these processes have been targeted therapeutically with little effect. For example, despite the well-characterized role of ROS overproduction in doxorubicin cardiotoxicity, clinical trials testing the common antioxidants N-acetylcysteine and α-tocopherol have not demonstrated a significant cardioprotective effect in patients (5, 6), suggesting that ROS may not be the only inciting factor responsible for doxorubicin cardiomyopathy.

Currently, dexrazoxane is the only FDA-approved drug used clinically to prevent doxorubicin-induced heart failure. It is believed to chelate intracellular iron and block iron-assisted oxidative radical production (7, 8). Dexrazoxane may also protect cardiac cells by inhibiting topoisomerase IIβ, which has recently been implicated in the pathogenesis of doxorubicin cardiotoxicity (9, 10). However, in practice the use of dexrazoxane is limited because of concerns that it may interfere with doxorubicin's ability to kill tumor cells (11). In addition, dexrazoxane has been reported to induce secondary malignancies (12), which has led to its removal from the market in Europe. As such, new approaches to cardioprotection are needed.

Zebrafish have been used successfully for high-throughput screening (HTS) to identify chemical compounds that suppress genetic defects and other disease states (13–15). Compared to cell-based *in vitro* systems, *in vivo* screening offers several advantages, including the ability to discover compounds with therapeutic activity even without knowing

their molecular targets. In addition, compounds discovered by *in vivo* screening are selected for their ability to be effective in the complex context of the disease of interest. We therefore sought to establish a zebrafish model of doxorubicin-induced cardiomyopathy that we could use to screen for new cardioprotective compounds.

## Results

### A doxorubicin-induced cardiomyopathy model in zebrafish

To avoid interference with the early cardiogenic process, we started to treat zebrafish 1 day post-fertilization (dpf), after the heart had formed and circulation had begun. We treated animals with 100 μM doxorubicin and assessed phenotypic changes at 3 dpf (Fig 1A). Two days after doxorubicin exposure, fish exhibited extensive pericardial edema. Microscopic examination revealed that the heart atrium was elongated and the ventricle collapsed (Fig 1B). Heart contraction was dramatically compromised, resulting in the absence of blood cell circulation within tail blood vessels (Movie S1 and S2). Using a high-speed camera and a custom analysis algorithm (16), we calculated the fractional shortening of the zebrafish hearts. Both heart rate and contractility were dramatically reduced in doxorubicin-treated fish (Fig 1C, F). We used a transgenic zebrafish line Tg(myh7:dsRed) which expresses the fluorescent protein dsRed from the beta-myosin heavy chain promoter, to visualize individual cardiomyocytes We found that both atrium and ventricle cardiomyocyte numbers were significantly reduced compared to controls (Fig 1D, G). TUNEL staining also showed that doxorubicin increased cardiomyocyte apoptosis (Fig 1E, H). Therefore, the zebrafish model appeared to recapitulate several key aspects of doxorubicin-induced cardiomyopathy in humans, including increased apoptosis and reduced contractility. Because the doxorubicin-induced changes in cardiac function and blood circulation were easily detected visually, we used them to form the basis of an assay to screen for small molecules that suppressed doxorubicin-induced cardiotoxicity.

### Identification of compounds that prevent doxorubicin-induced cardiomyopathy in zebrafish

We screened 3,000 small molecules from the Prestwick and Spectrum chemical libraries and identified eight compounds that were capable of preventing doxorubicin-induced decreases in cardiac contraction and circulation. Two particularly potent agents, visnagin (VIS) and diphenylurea (DPU), were protective at concentrations below 1μM (Fig 1I, J). VIS, a furanochromone, and DPU, a urea derivative, belong to distinct structural classes. Three of the six less potent effective molecules shared clear structural similarity with VIS, confirming the efficacy of this structural class in reversing doxorubicin cardiotoxicity. VIS and DPU prevented the overt morphological effects of doxorubicin on the heart, including ventricular compaction and pericardial edema (Fig 1K, L; Movie S3). Both compounds completely rescued cardiac contractility, as measured by fractional shortening (Fig 1M, N). VIS and DPU represent two distinct compound classes that potently protect the heart from the toxic effects of doxorubicin.

### VIS and DPU reduce doxorubicin-induced cardiac cell death in vitro and in vivo

Because cardiomyocyte apoptosis contributes to doxorubicin-induced cardiomyopathy, we determined whether VIS and DPU attenuated heart failure by inhibiting cardiomyocyte apoptosis. We first tested whether VIS and DPU attenuate doxorubicin-induced cell death of neonatal rat cardiomyocytes (NRCM) by TUNEL assay and Annexin-V staining. Both VIS and DPU significantly decreased doxorubicin-induced cell death (Fig 2A, B). Moreover, VIS and DPU also reduced doxorubicin cell death of a cardiac cell line HL1 (Fig 2C) and consistently enhanced cell survival after doxorubicin treatment (Fig 2D). Furthermore, we tested if VIS and DPU inhibit cell death in doxorubicin-treated zebrafish and mice *in vivo*. In a transgenic zebrafish line expressing nuclear DsRed from the myl7 promoter in cardiomyocytes, we performed TUNEL staining to identify apoptotic cells after treatment with doxorubicin. Doxorubicin treatment caused a 4-fold increase in apoptotic cardiomyocytes in zebrafish 4 days after fertilization. VIS and DPU reduced the cardiomyocyte apoptotic index almost to the baseline level (Fig 2E).

To determine if the ability of VIS and DPU to protect cardiomyocytes from apoptosis was conserved in mammals, we treated mice with doxorubicin with or without co-treatment with VIS or DPU. One day later, hearts were collected for apoptosis assays with TUNEL. As seen in zebrafish, doxorubicin caused a 3- to 4-fold increase in apoptosis in mouse cardiac sections. Co-treatment with VIS or DPU significantly decreased doxorubicin-induced apoptosis (Fig 2F). Furthermore, we tested the cardioprotective effect of VIS by *ex vivo* imaging with an Annexin V conjugate with a near infrared fluorochrome, Annexin-Vivo-750 (AV-750) (17). The result confirmed that VIS significantly reduced doxorubicin-induced apoptosis in mouse hearts (Fig 2G). Therefore, VIS and DPU prevented doxorubicin-induced cardiac apoptosis in both zebrafish and mice.

Because published reports have implicated ROS production in the pathogenesis of doxorubicin cardiotoxicity, we tested hydrogen peroxide ($H_2O_2$) levels with CM-H2DCFDA staining in HL-1 cultured cardiomyocytes. We observed an increase in $H_2O_2$ levels with doxorubicin treatment that was not affected by the addition of either VIS or DPU (Fig. S1), suggesting that attenuation of $H_2O_2$-associated oxidative stress is not a key mechanism of cardioprotection with these agents.

### VIS improves cardiac function in doxorubicin-treated mice

To determine if the in vivo cardioprotective effect is conserved across species, we employed two murine models of doxorubicin-induced cardiomyopathy. Because of the costs associated with testing two cardioprotectant compounds, we focused only on VIS for these studies. We induced acute cardiomyopathy by injecting mice with 15 mg/kg doxorubicin intraperitoneally, and injected 25 mg/kg VIS or vehicle immediately prior to doxorubicin injection. Five days after the initial injection, we assessed cardiac function by echocardiography and found that mice treated with doxorubicin and VIS exhibited significantly better fractional shortening and strain rate than did mice treated with doxorubicin alone (Fig 3A–C, Table 1). Similarly, we induced cardiomyopathy by repeated injection of low dosage doxorubicin for five weeks (5mg/kg/week) followed by an additional seven weeks without doxorubicin (18). VIS significantly improved cardiac

function after doxorubicin treatment in this chronic model, as measured by fractional shortening and strain rate (Fig 3D–F, Table 2).

### VIS binds to MDH2

To identify the cardioprotective target of VIS, we performed a structure-activity relationship study of VIS and found that bergapten, a psoralen compound found in grapefruit juice, was a potent structural analog. We then synthesized a derivative of bergapten that possessed an alkyl linker capable of being attached to a solid support (Fig 4A). Affinity chromatography of whole zebrafish lysates followed by silver staining revealed a single band that bound to bergapten-coupled beads. This binding was inhibited by free VIS (Fig 4B). Mass spectrometry analysis identified the protein as mitochondrial malate dehydrogenase (MDH2). The specific binding of MDH2 to the affinity beads was further confirmed by Western blotting with an anti-MDH2 antibody (Fig 4C).

### Effect of MDH2 inhibition and L-malic acid on doxorubicin cardiotoxicity

To determine whether MDH2 inhibition was responsible for the cardioprotective effect of VIS, structurally diverse MDH2 inhibitors were selected from the published literature and tested for their ability to protect the heart from doxorubicin (19, 20). In cultured HL1 cells, mebendazole, thyroxine (T4), and iodine all increased cardiomyocyte viability compared to doxorubicin treatment alone (Fig 4D). Furthermore, co-treatment with any of these MDH2 inhibitors rescued zebrafish from doxorubicin-induced cardiotoxicity or death (Fig 4E). Moreover, coadministration of L-malic acid protected the fish from development of the doxorubicin cardiotoxic phenotype in a dose-dependent fashion (Fig 4F). Therefore, inhibition of MDH2 or exogenous augmentation of malate concentrations is sufficient to protect cardiac cells from doxorubicin toxicity.

### Inhibition of the malate-aspartate shuttle protects against doxorubicin cardiotoxicity

In addition to its role in the TCA cycle, MDH2 is one of the key enzymes in the malate-aspartate shuttle (MAS). Because the inner mitochondrial membrane is impermeable to NADH, the MAS is the primary mechanism by which electrons are transported across the mitochondrial membrane in the mammalian heart. To test the hypothesis that MDH2 inhibition confers its cardioprotective effects through inhibition of the MAS, we treated zebrafish embryos with doxorubicin and the MAS inhibitor aminooxyacetate (AOA). Coadministration of AOA protected fish from the development of doxorubicin cardiotoxicity in a dose-dependent manner (Fig 4G) similarly to VIS, suggesting that VIS's cardioprotective effects may be related to MAS inhibition.

### Neither VIS nor DPU protects tumor cells in vitro or in vivo

The goal of the preceding studies was to identify compounds capable of reducing doxorubicin's cardiotoxicity but preserving its anti-tumor potency. Thus, we next determined whether VIS or DPU protects tumor cells from doxorubicin-mediated cell death. We tested whether VIS or DPU at concentrations up to 50 μM protected several solid tumor lines from doxorubicin-induced cell death, including two prostate tumor lines DU145 and

LNCaP and two breast cancer lines MCF7 and MDA-MB-231. We found that VIS and DPU did not increase cell survival of any of the lines after doxorubicin treatment (Fig 5A–D).

We then determined whether VIS or DPU reduced the chemotherapeutic efficacy of doxorubicin *in vivo*. To this end, we utilized a zebrafish xenograft system in which Jurkat T-ALL leukemia cells were transplanted to zebrafish *in vivo.* We treated the recipient animals with doxorubicin with or without VIS or DPU. Doxorubicin effectively reduced the burden of T-ALL cells in zebrafish. Co-treatment with VIS or DPU caused no reduction in doxorubicin's efficacy (Fig 5E).

In addition, we tested VIS in a murine model in which MDA-MB-231 breast cancer cells had been transplanted into the mammary fat pad of NSG (NOD.Cg-Prkdc$^{scid}$ Il2rg$^{tm1Wjl}$/SzJ) mice to generate xenograft tumors. Two weeks after initial cell implantation, mice were treated with vehicle, doxorubicin, or doxorubicin plus VIS, and the tumor size was assessed by caliper measurement throughout the experimental period from 0 to 20 days post-treatment. Doxorubicin effectively reduced the mammary tumor burden in mice. VIS did not interfere with doxorubicin's efficacy (Fig 5F), which was further confirmed by weighing tumors post mortem from different groups (Fig 5G,H). Taken together, these results indicate that VIS and DPU are effective cardioprotectants that do not interfere with doxorubicin's activity against a variety of cancer cell types.

## Discussion

By establishing a doxorubicin-induced cardiomyopathy model in zebrafish, we conducted target-naïve, phenotype-based screening of a chemical library to identify newly described cardioprotective compounds. Two compounds, VIS and DPU, attenuate cardiac cell death and preserve cardiac function in zebrafish and mice. VIS and DPU do not interfere with doxorubicin-induced tumor cell death, underscoring the likelihood that the beneficial and detrimental effects of doxorubicin can be separated pharmacologically.

Neither VIS nor DPU has been previously linked to doxorubicin toxicity or heart failure. VIS is a natural product biosynthesized by the toothpickweed *Ammi visnaga* (21). Several previous papers have suggested a cell-protective effect for VIS. It has been reported that VIS can protect kidney epithelial cells from damage by oxalate and protect neurons from kainic acid-induced apoptosis (22, 23). Furthermore, VIS has been shown to inhibit LPS-stimulated inflammation in a microglial cell line (24). Very little is known about the biological function and target of DPU.

Using an affinity chromatography approach, we discovered that VIS binds to mitochondrial malate dehydrogenase. We observed cardioprotection with the administration of other MDH2 inhibitors as well as with malic acid itself, suggesting that modulation of MDH2 may underlie VIS's therapeutic effect. For both iodine and thyroxine, a hint of cardioprotection can be found in the literature. Iodine has been shown to improve the antineoplastic effects of doxorubicin and simultaneously attenuate doxorubicin cardiotoxicity in a rat breast cancer model, although MDH2 was not hypothesized as a mechanism (25). Similarly, heart-specific expression of human type 2 iodothyronine deiodinase in transgenic mice leads to elevated

levels of thyroid hormone in the heart and improved cardiac function when exposed to doxorubicin (26). Mebendazole has no known role in cardioprotection but nonetheless rescued the cardiomyopathy phenotype in our zebrafish model. It should be noted that iodine, thyroxine, and mebendazole are non-specific compounds that modulate many targets, which may explain their reduced efficacy and increased toxicity relative to VIS. In summary, these structurally diverse MDH2 inhibitors mimic VIS's protective effects and suggest that MDH2 inhibition is sufficient to protect the heart from doxorubicin.

A major unanswered question is how MDH2 inhibition can be protective in cardiac cells without protecting cancer cells from doxorubicin. One possibility is that doxorubicin damages cardiac and cancer cells through different mechanisms, and that MDH2 inhibition interferes with the cardiac-specific mechanism. Although doxorubicin and the anthracyclines have been in clinical use for decades, it remains unclear how they induce cell death and whether they cause cell death through shared or distinct pathways in cardiac and cancer cells. Extensive studies have documented that doxorubicin triggers a number of cellular events including DNA damage and oxidative stress (3), and one or more of these processes may be a more significant contributor to cell death in the heart than in a tumor. For example, it is possible that VIS modulates metabolic pathways that differentially contribute to the injury response in minimally proliferating cardiomyocytes and rapidly proliferating tumor cells, thereby preventing a maladaptive response to injury specifically in cardiomyocytes.

One intriguing possibility is the involvement of the malate-aspartate shuttle (MAS) used to traffic reducing equivalents between mitochondria and the cytosol. Enzymes of the TCA cycle have been shown to physically interact with MAS enzymes, allowing for direct communication of metabolic changes between the mitochondrial matrix and the cytosol (27). The TCA cycle is thought to function similarly in zebrafish and humans (28, 29). Moreover, the amino acid sequences for the MAS enzymes MDH2 and aminoaspartate transferase share between 79% and 85% homology between zebrafish and humans, suggesting similar roles of these metabolic pathways across species (30). It has been proposed that MAS inhibition in cardiac cells decreases mitochondrial respiration prior to cardiac injury, thereby minimizing oxidative damage during recovery in a process that mimics ischemic preconditioning(31). In contrast, tumor cells rely primarily on aerobic glycolysis rather than mitochondrial respiration via the well-characterized Warburg effect(32). Thus, it is conceivable that MAS inhibition may protect against a cardiotoxic injury without significantly affecting tumor metabolism and growth.

As with many animal studies, our study is limited by the challenges in translating findings in zebrafish and rodent models to the delayed-onset chronic cardiomyopathy seen in patients treated with doxorubicin. Prior to clinical use of the cardioprotective compounds identified in our screen, further experiments are needed to test different routes of administration, document any long-term toxicities, and confirm efficacy in preventing the development of cardiomyopathy. In addition, we tested a limited number of tumor cell lines and xenograft models, and it is unclear whether the preservation of doxorubicin's anti-tumor activity would extend to all types of malignancy. A more detailed characterization of the

mechanisms behind MDH2-mediated cardioprotection may facilitate our understanding of the role of this pathway in cancer cell survival and growth.

Although much remains to be learned about the mechanisms by which VIS and DPU provide cell type-specific protection from doxorubicin, their discovery offers compelling evidence that doxorubicin-induced cell death can be mitigated in a cell-specific fashion. Moreover, the discovery that MDH2 inhibition is sufficient for cardioprotection provides not only a potential new therapeutic target, but also a new entrance point for investigating the fundamental differences of responsiveness to doxorubicin by cardiac and tumor cells. Future experiments will focus on elucidating the role of MDH2 in doxorubicin's chemotherapeutic and cardiotoxic mechanisms. In addition, it will be informative to determine whether visnagin's cardioprotective effects extend to other modes of cardiac injury, such as ischemia-reperfusion or other cardiotoxic chemotherapies.

## Materials and Methods

### Study Design

High-throughput chemical screening was performed in zebrafish embryos to identify novel therapies for doxorubicin-induced cardiotoxicity. Screen hits were confirmed in zebrafish embryos by measuring cardiomyocyte number, apoptosis, and fractional shortening; in male C57BL/6 mice by measuring TUNEL staining, Annexin V whole organ staining, and echocardiographic fractional shortening and strain rate; and in cultured HL1 cells by measuring cell viability and Annexin V staining. The target of visnagin was identified using affinity chromatography and mass spectrometry analysis followed by confirmatory Western blot. Finally, screen hits were tested in zebrafish and mouse xenograft tumor models as well as in DU145, LNCaP, MCF7, and MDA-MB-231 tumor cell lines.

For mouse studies, sample size was selected based on published data. Zebrafish cardiac function data and mouse echocardiographic data were analyzed by a study author blinded to the treatment conditions. All animals were randomly assigned to treatment groups for zebrafish cardiomyocyte counting, cardiac apoptosis, fractional shortening, and MDH2 inhibitor experiments, as well as for mouse cardiac apoptosis, Annexin V staining, cardiac function assessment, and xenograft tumor experiments. Given the small size of these studies and similar genetic background of the animals in each group, no formal randomization protocol was utilized.

### Animals

All zebrafish and mouse experiments were reviewed and approved by the MGH Institutional Animal Care and Use Committee or the Dalhousie University Care of Laboratory Animals Committee.

### Zebrafish model

Myl7-EGFP fish embryos (33) (1 dpf) were arrayed into 96-well plates, with each well containing three fish in 200 μl E3 buffered with HEPES (pH 7.2) with 100 μM doxorubicin. For screening, about 400nL of small molecule stock solution (in DMSO) was transferred

from 96-well format library plates to the screening plates in the presence of iron (either using a stainless steel pin tool or through supplementation with ferric chloride 10 μM). At 3 dpf, treated fish were screened with an inverted fluorescent microscope (100×) for heart contraction and tail circulation.

### Cell Culture

Neonatal rat cardiomyocytes were isolated from postnatal day 1 rats with a Neonatal Cardiomyocyte Isolation Kit (Worthington Biochemical) following manufacturer's instruction, and cultured with L-15 medium.

Cardiac cell line HL-1 was derived from mouse atrium tumor and was a generous gift from Dr. William Claycomb. Culturing conditions were previously published (34). In brief, HL-1 cells were cultured with Claycomb medium (Sigma) supplemented with fetal bovine serum (FBS), penicillin/ streptomycin, L-glutamine and norepinephrine.

DU145 and LNCaP are human prostate tumor lines, while MCF7 and MDA-MB-231 are human breast cancer lines. DU145, MCF7 and MDA-MB-231 cells were cultured with high glucose DMEM (Life Sciences) supplemented with penicillin/streptomycin and L-glutamine, and LNCaP was grown in RPMI-1640 (Life Sciences) plus penicillin/ streptomycin and L-glutamine.

### Reagents

The Spectrum and Prestwick libraries were purchased from MicroSource Discovery Systems, Inc. and Prestwick Chemical, respectively. Doxorubicin, visnagin, diphenylurea, mebendazole, L-thyroxine, iodine, L-malic acid, and aminooxyacetic acid hemihydrochloride were obtained from Sigma-Aldrich. If not specified, all chemicals were dissolved in DMSO. The only exceptions were that doxorubicin was dissolved in saline and VIS was dissolved in vehicle containing 10% ethanol and 90% olive oil when injected into mice for the cardiac function and xenograft tumor studies.

### Zebrafish cardiomyocyte counting

Myl7-nuc-dsRed fish (1 dpf) were treated with DMSO or 100 μM doxorubicin for two days (n=5 each). Hearts were surgically removed and fixed with 4% paraformaldehyde (PFA) for 20 minutes at room temperature. The fixed heart samples were embedded in mounting medium and flattened with slide and coverslip. Confocal images were captured from the flattened hearts, and red nuclei were counted.

### Zebrafish cardiac apoptosis assay

Myl7-nuc-dsRed fish larvae (1 dpf) were treated with DMSO, 100 μM doxorubicin or doxorubicin plus 20 μM rescue compounds for two days (n=5 each). Hearts were surgically removed and fixed with 4% PFA for 20 minutes at room temperature. After staining with an *in situ* TUNEL kit (Roche), heart samples were embedded in mounting medium, flattened with slide and coverslip, and then subjected to confocal microscopy. The data were quantified as percentage of TUNEL positive cardiomyocytes.

### Zebrafish heart fractional shortening measurement

Zebrafish (1 dpf) were treated with DMSO, doxorubicin, doxorubicin + VIS, or doxorubicin + DPU for two days (n=13–19 each). High speed video microscopy and measurement of ventricular size and function were performed as previously described(16). Briefly, M-mode images were assembled from sequential frames across a fixed scan line. Ventricular size was determined by measurement across endocardial borders at end systole and diastole, and fractional shortening was calculated.

### Mouse cardiac apoptosis

Male C57BL/6 mice between 8–10 weeks were injected with DMSO, 15 mg/kg doxorubicin, or doxorubicin plus 25 mg/kg visnagin or 10 mg/kg diphenylurea intraperitoneally (n=4–5 each). One day after injection, hearts were collected and fixed with 4% PFA at 4°C overnight and then were subjected to paraffin embedding and sectioning. The heart sections were stained using the TMR TUNEL kit (Roche) following the manufacturer's protocol. The stained sections were scanned with MetaMorph-assisted slide scanning microscopy, and apoptosis indices were quantified as TUNEL positive cell/$mm^2$.

### Cell viability assay

Cultured HL1 and DU145 cells were treated with doxorubicin for the indicated amounts of time and were assayed using CellTiter Glo Luminescent Cell Viability Assay (Promega).

### Cell Hydrogen Peroxide ($H_2O_2$) detection

$H_2O_2$ production was assessed by CM-H2DCFDA (Invitrogen) staining as previously described (35). Briefly, cultured HL-1 cells were treated with doxorubicin with or without VIS, DPU or the general antioxidant scavenger 2-mercaptopropionyl-glycine (MPG) for 8 hours and then stained with 10mM CM-H2DCFDA followed by confocal microscopy (excitation/emission, 490/525nm).

### AnnexinV staining

Neonatal rat cardiomyocytes and HL1 cells were stained with fluorescent Annexin V (Roche) and were live imaged after being treated with doxorubicin for the indicated amounts of time. Apoptosis indices were quantified as percentage of AnnexinV positive cells.

Whole organ staining was performed using an Annexin V conjugate with a near infrared fluorochrome, Annexin-Vivo-750 (AV-750) (PerkinElmer Life Sciences). Three cohorts of male C57BL/6 mice between 8 to 10 weeks of age (n=5 each) were compared: untreated control, doxorubicin treatment, doxorubicin and VIS co-treatment. 20 hr post treatment, mice were injected intravenously with 100 μl of AV-750. Four hours later, the mice were sacrificed according to the approved animal protocol and the heart was imaged immediately in its short axis using a commercial imaging system (IVIS Spectrum, PerkinElmer). AV-750 fluorescence was detected with an excitation wavelength of 745 nm/emission wavelength of 800 nm, a 30-sec exposure time and a spatial resolution of 135 μm. Fluorescence standards of serially diluted AV-750 were imaged simultaneously, enabling calibration of the acquired

signal. Total fluorescence within the left ventricle was quantified and normalized to the control mice.

### Mouse cardiac function assessment

C57BL/6 male mice between 8–10 weeks of age were purchased from Charles River Laboratories and randomly grouped (n= 4–8). An acute heart failure model was generated by a single intraperitoneal (IP) injection of 15 mg/kg doxorubicin dissolved in saline, while the chronic model involved IP injection of 5 mg/kg doxorubicin weekly for 5 consecutive weeks. In the treatment group, 25mg/kg visnagin was dissolved in vehicle consisting of 10% ethanol and 90% olive oil, and then injected IP immediately followed by contralateral doxorubicin injection. In the control group, plain vehicle and saline were injected instead. Five days (for the acute model) or twelve weeks (for the chronic model) after treatment, transthoracic echocardiographic images were obtained and interpreted by an echocardiographer blinded to the experimental design using a 13.0-MHz linear probe (Vivid 7; GE Medical System, Milwaukee, WI) as described previously (36, 37). Briefly, mice were lightly anesthetized with ketamine (20 mg/kg). M-mode images were obtained from a parasternal short-axis view at the midventricular level with a clear view of the papillary muscle. Tissue Doppler imaging was collected at a frame rate of 483 frames per second and a depth of 1 cm. LV end-diastolic internal diameter (LVIDd) and LV end systolic internal diameter (LVIDs) were measured. Fractional shortening (FS) was defined as [(LVIDd − LVIDs)/LVIDd] × 100. Strain rate of the posterior wall was analyzed offline in an EchoPAC workstation (GE Healthcare, Wauwatosa, WI). In brief, a region of interest (axial distance, 0.2 mm; width, 0.6 mm) was manually positioned in the middle of the posterior wall. A strain length of 0.5 mm was used. Peak systolic strain rate was measured. The temporal smoothing filters were turned off for all measurements. The values of three consecutive cardiac cycles were averaged.

### Procedure for immobilizing bergapten derivative to affinity chromatography matrix

Bergapten was identified as a potent structural analog of visnagin. A bergapten derivative was synthesized via demethylation and alkylation of commercially available bergapten (Sigma-Aldrich) and coupled to Affi-Gel 10 affinity chromatography matrix.

Synthesis of 4-hydroxy-7*H*-furo[3,2-*g*]chromen-7-one 3: $BBr_3$ (8 mL, 8 mmol, 1 M in dichloromethane) was added dropwise to a solution of bergapten (432 mg, 2 mmol) in dichloromethane (8 mL) and the solution stirred at 0°C for 2 hrs. After completion of the reaction, saturated $NaHCO_3$ solution was poured slowly into the solution resulting in the precipitation of a solid. The product was recovered by filtration, washed with cold water and ether and dried under a high vacuum, yielding compound **3** as a white solid (303 mg, 1.50 mmol, 75%). $^1$H NMR (500 MHz, $d_6$-DMSO) δ 11.35 (br, 1H), 8.23 (d, J = 9.5 Hz, 1H), 7.88 (d, J = 2.0 Hz, 1H), 7.17 (d, J = 2.5 Hz, 1H), 7.12 (s, 1H), 6.23 (d, J = 9.5 Hz, 1H); EI-MS m/z 202 ($M^+$).


2 3

Synthesis of *tert*-butyl (3-((7-oxo-7*H*-furo[3,2-*g*]chromen-4-yl)oxy)propyl)carbamate 4: Compound **3** (40 mg, 0.2 mmol), 3-(Boc-amino)propyl bromide (48 mg, 0.2 mmol), and potassium carbonate (42 mg, 0.3 mmol) were mixed in dimethylformamide (DMF) (1 mL). The reaction mixture was heated under reflux until TLC analysis (EA:Hex=1:1, $R_f$ = 0.4) confirmed that the reaction was complete. Water was added and the mixture was extracted with ethyl acetate. The combined organic extracts were washed with brine, dried over $Na_2SO_4$, and the solvent was removed in vacuo. The residue was purified via column chromatography, yield 90% (65mg, 0.18 mmol). $^1$H NMR (500 MHz, $CDCl_3$) δ 8.16 (d, J = 9.5 Hz, 1H), 7.59 (d, J = 4.5 Hz, 1H), 7.26 (d, J = 6.5 Hz, 1H,), 7.15 (d, J = 6.5 Hz, 1H), 6.99 (s, 1H), 6.29 (d, J = 9.5 Hz, 1H), 4.52 (t, J = 6.0 Hz, 2H), 3.41 (t, J = 5.0 Hz, 2H,), 2.12–2.05 (m, 2H), 1.46 (s, 9H); ESI-MS m/z 359.7 ($M^+$).

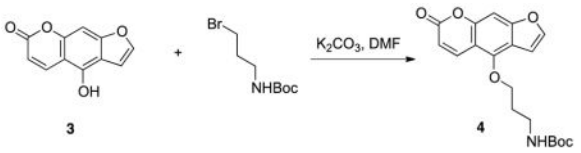


3 4

Synthesis of 4-(3-aminopropoxy)-7*H*-furo[3,2-*g*]chromen-7-one 5: To a stirring solution of compound **4** (36mg, 0.1 mmol) in dry $CH_2Cl_2$ (1 mL) at 0°C, trifluoroacetic acid (0.1 mL) was slowly added and the reaction mixture was stirred 1 hour at room temperature. The mixture was concentrated under vacuum. The residue was suspended in ethyl acetate (10 mL) and a saturated $NaHCO_3$ solution was added to adjust the pH to 7 at 0 °C. The mixture was extracted with ethyl acetate (3 ×10 mL). The combined organic layer was dried over $Na_2SO_4$, filtered and concentrated in vacuo. The crude product was used without further treatment, yield 95% (25mg, 0.095 mmol). $^1$H NMR (500 MHz, $CDCl_3$) δ 8.15 (d, J = 10.0 Hz, 1H), 7.59 (d, J = 2.0 Hz, 1H), 7.15 (s, 1H), 7.01–6.99 (m, 1H), 6.27 (d, J = 9.5 Hz, 1H), 6.29 (t, J = 9.5 Hz, 1H), 4.55 (t, J = 6.0 Hz, 2H), 2.99 (t, J = 7.0 Hz, 2H,), 2.04–2.00 (m, 2H); ESI-MS m/z 259.8 ($M^+$).

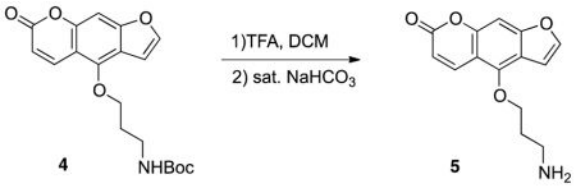


4 5

Coupling of bergapten derivative to immobilized agarose bead 1: Compound **4** (5mg, 0.02mmol), 1 mL agarose beads (Affi-Gel 10; Biorad, 0.015mmol/mL) washed thoroughly with anhydrous DMSO, and N,N-diisopropylethylamine (6μL, 0.03mmol) were mixed in 1 mL anhydrous DMSO. The mixture was rotated 8 hrs at room temperature. The resulting

slurry was drained and the beads were washed with water and DMSO. Bergapten-coupled agarose beads were stored in DMSO at 4°C.

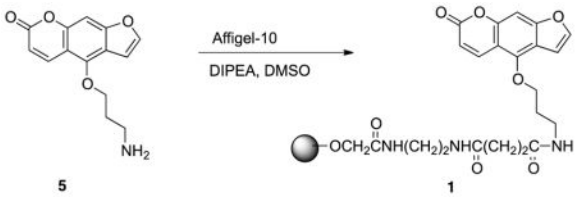


5 1

## Affinity Chromatography

Prior to chromatography, control and bergapten-coupled Affi-Gel matrix was blocked with 2 mg/mL bovine serum albumin (BSA) and 1% goat serum overnight at 4°C. 0.2% sodium azide was added as an antimicrobial. Zebrafish larvae were homogenized in lysis buffer (10 mM Tris [pH 7.4]; 150 mM NaCl; 1 mM $CaCl_2$; 1% Triton X-100; supplemented with protease inhibitor cocktail and phosphatase inhibitor) at 72 hours post-fertilization using a motorized pestle. The homogenate was centrifuged for 10 minutes at 14,000g at 4°C. The supernatant was removed and diluted to a final protein concentration of 6 mg/mL. Control and bergapten-coupled matrix was suspended in phosphate buffered saline (PBS) and incubated with the tissue lysate for two hours at 4°C. The supernatant was removed and the matrix was washed four times with lysis buffer. The matrix was then incubated with visnagin 500 μM (competitive elution) or an equivalent volume of DMSO (control elution) for two hours at 4°C. After removal of the supernatant, the matrix was serially washed with lysis buffer containing either visnagin 500 μM or an equivalent volume of DMSO (half-hour incubation per wash). Protein bound to the matrix was denatured with sample buffer prior to gel electrophoresis. Total protein lysate was diluted 10-fold in lysis buffer and similarly denatured prior to gel electrophoresis.

## Silver Stain and Mass Spectrometry Analysis

Equal quantities of protein were resolved on a 10% NuPage Bis-Tris gel. Silver staining was performed using a kit according to the manufacturer's protocol (Invitrogen). The band of interest was excised from the silver stained gel and analyzed via liquid chromatography-tandem mass spectrometry (LC/MS-MS; Taplin facility, Harvard Medical School). The excised gel band was cut into pieces and subjected to a modified in-gel trypsin digestion procedure(38) using a 50 mM ammonium bicarbonate solution containing 12.5 ng/μl modified sequencing-grade trypsin (Promega, Madison, WI) at 4°C. A nano-scale reverse-phase HPLC capillary column was created as described(39). Each sample was loaded onto the column via a Famos auto sampler (LC Packings, San Francisco CA). As peptides eluted, they were subjected to electrospray ionization and entered into an LTQ Orbitrap Velos Pro ion-trap mass spectrometer (ThermoFisher, San Jose, CA). Peptide sequences (and hence protein identity) were determined by matching protein databases with the acquired fragmentation pattern by the software program Sequest (ThermoFisher, San Jose, CA).(40) Spectral matches were manually examined and multiple identified peptides per protein were required.

### Western Blot Confirmation of Target Identity

Affinity chromatography with competitive elution was performed as described. Following SDS-PAGE, proteins were transferred to a polyvinylidene difluoride membrane (Bio-Rad), blocked with 5% BSA, and incubated with anti-MDH2 antibody (Sigma-Aldrich) at 4 °C overnight. Immunodetection was performed using a mouse anti-rabbit IgG light-chain specific secondary antibody (Jackson ImmunoResearch) and Amersham ECL Prime Western Blotting Detection Reagent (GE Healthcare Life Sciences).

### MDH2 Inhibitor, L-Malic Acid, and Aminooxyacetate Treatment

HL-1 cardiomyocytes and Tubingen AB (TuAB) zebrafish embryos at 30 hours post-fertilization were treated with doxorubicin 100 μM and one of several MDH2 inhibitors, L-malic acid, or aminooxyacetate. The highest non-toxic dose was chosen for each MDH2 inhibitor (mebendazole: 6.25 μM in cultured cells and 1 μM in zebrafish; thyroxine: 100 μM in both cultured cells and zebrafish; iodine: 200 μM in cultured cells and 100 μM in zebrafish). 150 zebrafish embryos were treated for each condition. Assessment of phenotype was performed 28 hours after treatment in cultured cells and 48 hours after treatment in zebrafish.

### Xenograft Tumor Models

**Mouse—**Six-week old female NSG (NOD.Cg-Prkdcscid Il2rgtm1Wjl/SzJ) mice (Jackson Laboratory) were anesthetized with isofluorane. $1\times10^6$ MDA-MB-231 cells in 100ul of 1:1 PBS and Matrigel (BD) were injected into the $4^{th}$ right mammary fat pad. Two weeks after tumor cell implantation, mice were randomly grouped (n=8 each) and treated once a week for two weeks (day 0 and day 7) with vehicle, doxorubicin (2mg/kg body weight) or doxorubicin (2mg/kg body weight) + visnagin (20mg/kg body weight).

**Zebrafish—**Mutant *casper* zebrafish embryos (41) at 24 hours post-fertilization (hpf) were anesthetized with 0.090 mg/mL Tricaine (Sigma-Aldrich) and used for cell transplantation using a protocol adapted from Haldi et al., (2006) (42, 43). Briefly, CM-DiI-labeled leukemia cells were loaded into a pulled glass micropipette and approximately 50 cells were delivered, as a single injection, into the yolk sac of each embryo using a PLI-100A Pico-Liter Injector (Warner instruments). Following injection, embryos were allowed to recover at 28°C for 1 hour before transfer to 35°C where they remained for the experiment.

At 4 hours post-injection, only embryos with a uniform fluorescent cell mass at the site of injection were randomized and divided into four groups (n=15–20) for proliferation studies. Embryos xenotransplanted with human cancer cells were then treated with 100uM doxorubicin and 20uM VIS or DPU, and embryos were incubated for 48 hours until 72 hpf. Embryos treated with vehicle (0.1% DMSO) served as a negative control for drug efficacy(43).

For the fluorescence imaging, a filter with excitation/emission wavelengths of 550/605 nm was used and all embryos were photographed under the same settings. Groups of 15–20 xenografted embryos were dissociated into a single cell suspension and leukemia cells were enumerated by counting cells positive for PML bodies (found in human cells but not in

zebrafish cells). This was accomplished by performing cytospin (cytospin conditions: 300rpm for 10 minutes, using a Shandon cytospin 3 (Global Medical instrumentation)) of dissociated embryos, and immunohistochemistry for PML bodies (primary antibody: Rabbit Anti-PML (Santa Cruz sc-5621); secondary antibody: DyLight Donkey Anti-Rabbit IgG 649 (Abcam)). Fluorescent images were acquired on a custom built Zeiss Axio Observer Z1 inverted microscope equipped with 405 nm, 488 nm, 561 nm and 633 nm diode-based lasers (Intelligent Imaging Innovations (3i)) and a confocal spinning-disk unit (CSU-X1) (Yokagowa). Cells were observed using a 10× objective and images were recorded using an Evolve 512 electron-multiplying charge-coupled device (EMCCD) camera (Photometrics) and Slidebook 5.1 Software using the mosaic tool (Intelligent Imaging Innovations (3i)). The experiments were done three independent times.

### Statistical Analysis

For zebrafish cardiomyocyte counting, cell viability assay, and zebrafish and mouse cardiac apoptosis assays, experiments were performed at least three times and statistics were obtained by Student's T-test. For the *ex vivo* AnnexinV apoptosis assay, Annexin uptake was compared among the three groups of mice (Control vs. Dox vs. Dox+VIS) with one-way ANOVA and the Tukey post-test. Echo data was analyzed by one-way ANOVA with the Tukey post-test for the acute model or one-tailed T-test for the chronic model. Treatment with MDH2 inhibitors and L-malic acid in zebrafish was performed over five independent experiments and analyzed using two-tailed Student's T-test.

## Supplementary Material

Refer to Web version on PubMed Central for supplementary material.

## Acknowledgments

We thank W. C. Claycomb (LSU Health Sciences Center) for generously providing the HL1 cells. We are also grateful for the assistance in establishing mouse models of doxorubicin-induced cardiomyopathy by Drs. Kenneth D. Bloch and Marielle Scherrer-Crosbie at the MGH Cardiovascular Research Center.

**Funding:** YL and AA are supported by training grant T32HL007208 from the National Heart, Lung and Blood Institute. AA is supported by a John S. LaDue Memorial Fellowship. This work was supported by an Innovative Research Grant from the American Heart Association (IRG14600006 to RTP) and by the Charles and Ann Sanders MGH Research Scholar Award (to RTP). Daniel A. Haber and Min Yu are supported by the Howard Hughes Medical Institute. VLB is supported by a trainee award from the Beatrice Hunter Cancer Research Institute, with funds provided by the Canadian Imperial Bank of Commerce and Cancer Care Nova Scotia as part of The Terry Fox Strategic Health Research Training Program in Cancer Research at CIHR, and a trainee award from the Nova Scotia Health Research Foundation. Zebrafish xenograft studies were funded by a Canadian Institutes of Health Research and Natural Sciences and Engineering Research Council Collaborative Health Research Project awarded to GD and JNB.

## References and Notes

1. Suter TM, Ewer MS. Cancer drugs and the heart: importance and management. European heart journal. 2013; 34:1102–1111. [PubMed: 22789916]
2. Lipshultz SE, Cochran TR, Franco VI, Miller TL. Treatment-related cardiotoxicity in survivors of childhood cancer. Nature reviews Clinical oncology. 2013; 10:697–710.
3. Ky B, Vejpongsa P, Yeh ET, Force T, Moslehi JJ. Emerging paradigms in cardiomyopathies associated with cancer therapies. Circulation research. 2013; 113:754–764. [PubMed: 23989717]

4. Octavia Y, Tocchetti CG, Gabrielson KL, Janssens S, Crijns HJ, Moens AL. Doxorubicin-induced cardiomyopathy: from molecular mechanisms to therapeutic strategies. Journal of molecular and cellular cardiology. 2012; 52:1213–1225. [PubMed: 22465037]
5. Myers C, Bonow R, Palmeri S, Jenkins J, Corden B, Locker G, Doroshow J, Epstein S. A randomized controlled trial assessing the prevention of doxorubicin cardiomyopathy by N-acetylcysteine. Seminars in oncology. 1983; 10:53–55. [PubMed: 6340204]
6. Legha SS, Wang YM, Mackay B, Ewer M, Hortobagyi GN, Benjamin RS, Ali MK. Clinical and pharmacologic investigation of the effects of alpha-tocopherol on adriamycin cardiotoxicity. Annals of the New York Academy of Sciences. 1982; 393:411–418. [PubMed: 6959564]
7. Hasinoff BB, Herman EH. Dexrazoxane: how it works in cardiac and tumor cells. Is it a prodrug or is it a drug? Cardiovasc Toxicol. 2007; 7:140–144. [PubMed: 17652819]
8. Ichikawa Y, Ghanefar M, Bayeva M, Wu R, Khechaduri A, Naga Prasad SV, Mutharasan RK, Naik TJ, Ardehali H. Cardiotoxicity of doxorubicin is mediated through mitochondrial iron accumulation. The Journal of clinical investigation. 2014; 124:617–630. [PubMed: 24382354]
9. Lyu YL, Kerrigan JE, Lin CP, Azarova AM, Tsai YC, Ban Y, Liu LF. Topoisomerase IIbeta mediated DNA double-strand breaks: implications in doxorubicin cardiotoxicity and prevention by dexrazoxane. Cancer research. 2007; 67:8839–8846. [PubMed: 17875725]
10. Zhang S, Liu X, Bawa-Khalfe T, Lu LS, Lyu YL, Liu LF, Yeh ET. Identification of the molecular basis of doxorubicin-induced cardiotoxicity. Nature medicine. 2012; 18:1639–1642.
11. Swain SM, Whaley FS, Gerber MC, Weisberg S, York M, Spicer D, Jones SE, Wadler S, Desai A, Vogel C, Speyer J, Mittelman A, Reddy S, Pendergrass K, Velez-Garcia E, Ewer MS, Bianchine JR, Gams RA. Cardioprotection with dexrazoxane for doxorubicin-containing therapy in advanced breast cancer. Journal of clinical oncology : official journal of the American Society of Clinical Oncology. 1997; 15:1318–1332. [PubMed: 9193323]
12. Tebbi CK, London WB, Friedman D, Villaluna D, De Alarcon PA, Constine LS, Mendenhall NP, Sposto R, Chauvenet A, Schwartz CL. Dexrazoxane-associated risk for acute myeloid leukemia/myelodysplastic syndrome and other secondary malignancies in pediatric Hodgkin's disease. Journal of clinical oncology : official journal of the American Society of Clinical Oncology. 2007; 25:493–500. [PubMed: 17290056]
13. Le X, Pugach EK, Hettmer S, Storer NY, Liu J, Wills AA, DiBiase A, Chen EY, Ignatius MS, Poss KD, Wagers AJ, Langenau DM, Zon LI. A novel chemical screening strategy in zebrafish identifies common pathways in embryogenesis and rhabdomyosarcoma development. Development. 2013; 140:2354–2364. [PubMed: 23615277]
14. White RM, Cech J, Ratanasirintrawoot S, Lin CY, Rahl PB, Burke CJ, Langdon E, Tomlinson ML, Mosher J, Kaufman C, Chen F, Long HK, Kramer M, Datta S, Neuberg D, Granter S, Young RA, Morrison S, Wheeler GN, Zon LI. DHODH modulates transcriptional elongation in the neural crest and melanoma. Nature. 2011; 471:518–522. [PubMed: 21430780]
15. Peterson RT, Shaw SY, Peterson TA, Milan DJ, Zhong TP, Schreiber SL, MacRae CA, Fishman MC. Chemical suppression of a genetic mutation in a zebrafish model of aortic coarctation. Nature biotechnology. 2004; 22:595–599.
16. Shin JT, Pomerantsev EV, Mably JD, MacRae CA. High-resolution cardiovascular function confirms functional orthology of myocardial contractility pathways in zebrafish. Physiol Genomics. 2010; 42:300–309. [PubMed: 20388839]
17. Chen HH, Josephson L, Sosnovik DE. Imaging of apoptosis in the heart with nanoparticle technology. Wiley interdisciplinary reviews Nanomedicine and nanobiotechnology. 2011; 3:86–99. [PubMed: 20945336]
18. Hiona A, Lee AS, Nagendran J, Xie X, Connolly AJ, Robbins RC, Wu JC. Pretreatment with angiotensin-converting enzyme inhibitor improves doxorubicin-induced cardiomyopathy via preservation of mitochondrial function. The Journal of thoracic and cardiovascular surgery. 2011; 142:396–403 e393. [PubMed: 21094500]
19. Varrone S, Consiglio E, Covelli I. The nature of inhibition of mitochondrial malate dehydrogenase by thyroxine, iodine cyanide and molecular iodine. European journal of biochemistry / FEBS. 1970; 13:305–312. [PubMed: 4314809]

20. Tejada P, Sanchez-Moreno M, Monteoliva M, Gomez-Banqueri H. Inhibition of malate dehydrogenase enzymes by benzimidazole anthelmintics. Veterinary parasitology. 1987; 24:269–274. [PubMed: 3617430]

21. Kaul B, Staba EJ. Visnagin: biosynthesis and isolation from Ammi visnagi suspension cultures. Science. 1965; 150:1731–1732. [PubMed: 5858027]

22. Vanachayangkul P, Byer K, Khan S, Butterweck V. An aqueous extract of Ammi visnaga fruits and its constituents khellin and visnagin prevent cell damage caused by oxalate in renal epithelial cells. Phytomedicine. 2010; 17:653–658. [PubMed: 20036111]

23. Kwon MS, Lee JK, Park SH, Sim YB, Jung JS, Won MH, Kim SM, Suh HW. Neuroprotective Effect of Visnagin on Kainic Acid-induced Neuronal Cell Death in the Mice Hippocampus. Korean J Physiol Pharmacol. 2010; 14:257–263. [PubMed: 21165322]

24. Lee JK, Jung JS, Park SH, Park SH, Sim YB, Kim SM, Ha TS, Suh HW. Anti-inflammatory effect of visnagin in lipopolysaccharide-stimulated BV-2 microglial cells. Arch Pharm Res. 2010; 33:1843–1850. [PubMed: 21116788]

25. Alfaro Y, Delgado G, Carabez A, Anguiano B, Aceves C. Iodine and doxorubicin, a good combination for mammary cancer treatment: antineoplastic adjuvancy, chemoresistance inhibition, and cardioprotection. Molecular cancer. 2013; 12:45. [PubMed: 23705792]

26. Hong EG, Kim BW, Jung DY, Kim JH, Yu T, Seixas Da Silva W, Friedline RH, Bianco SD, Seslar SP, Wakimoto H, Berul CI, Russell KS, Lee KW, Larsen PR, Bianco AC, Kim JK. Cardiac expression of human type 2 iodothyronine deiodinase increases glucose metabolism and protects against doxorubicin-induced cardiac dysfunction in male mice. Endocrinology. 2013; 154:3937–3946. [PubMed: 23861374]

27. Beeckmans S, Kanarek L. Demonstration of physical interactions between consecutive enzymes of the citric acid cycle and of the aspartate-malate shuttle. A study involving fumarase, malate dehydrogenase, citrate synthesis and aspartate aminotransferase. European journal of biochemistry / FEBS. 1981; 117:527–535. [PubMed: 7285903]

28. Kanehisa M, Goto S. KEGG: kyoto encyclopedia of genes and genomes. Nucleic acids research. 2000; 28:27–30. [PubMed: 10592173]

29. Kanehisa M, Goto S, Sato Y, Kawashima M, Furumichi M, Tanabe M. Data, information, knowledge and principle: back to metabolism in KEGG. Nucleic acids research. 2014; 42:D199–205. [PubMed: 24214961]

30. Altschul SF, Madden TL, Schaffer AA, Zhang J, Zhang Z, Miller W, Lipman DJ. Gapped BLAST and PSI-BLAST: a new generation of protein database search programs. Nucleic acids research. 1997; 25:3389–3402. [PubMed: 9254694]

31. Nielsen TT, Stottrup NB, Lofgren B, Botker HE. Metabolic fingerprint of ischaemic cardioprotection: importance of the malate-aspartate shuttle. Cardiovascular research. 2011; 91:382–391. [PubMed: 21349875]

32. Warburg O. On respiratory impairment in cancer cells. Science. 1956; 124:269–270. [PubMed: 13351639]

33. Rottbauer W, Wessels G, Dahme T, Just S, Trano N, Hassel D, Burns CG, Katus HA, Fishman MC. Cardiac myosin light chain-2: a novel essential component of thick-myofilament assembly and contractility of the heart. Circ Res. 2006; 99:323–331. [PubMed: 16809551]

34. Claycomb WC, Lanson NA Jr, Stallworth BS, Egeland DB, Delcarpio JB, Bahinski A, Izzo NJ Jr. HL-1 cells: a cardiac muscle cell line that contracts and retains phenotypic characteristics of the adult cardiomyocyte. Proc Natl Acad Sci USA. 1998; 95:2979–2984. [PubMed: 9501201]

35. Korge P, Ping P, Weiss JN. Reactive oxygen species production in energized cardiac mitochondria during hypoxia/reoxygenation: modulation by nitric oxide. Circulation research. 2008; 103:873–880. [PubMed: 18776040]

36. Zou L, Feng Y, Chen YJ, Si R, Shen S, Zhou Q, Ichinose F, Scherrer-Crosbie M, Chao W. Toll-like receptor 2 plays a critical role in cardiac dysfunction during polymicrobial sepsis. Crit Care Med. 2010; 38:1335–1342. [PubMed: 20228680]

37. Neilan TG, Jassal DS, Perez-Sanz TM, Raher MJ, Pradhan AD, Buys ES, Ichinose F, Bayne DB, Halpern EF, Weyman AE, Derumeaux G, Bloch KD, Picard MH, Scherrer-Crosbie M. Tissue

Doppler imaging predicts left ventricular dysfunction and mortality in a murine model of cardiac injury. Eur Heart J. 2006; 27:1868–1875. [PubMed: 16717080]

38. Shevchenko A, Wilm M, Vorm O, Mann M. Mass spectrometric sequencing of proteins silver-stained polyacrylamide gels. Analytical chemistry. 1996; 68:850–858. [PubMed: 8779443]
39. Peng J, Gygi SP. Proteomics: the move to mixtures. Journal of mass spectrometry : JMS. 2001; 36:1083–1091. [PubMed: 11747101]
40. Eng JK, McCormack AL, Yates JR. An approach to correlate tandem mass spectral data of peptides with amino acid sequences in a protein database. Journal of the American Society for Mass Spectrometry. 1994; 5:976–989. [PubMed: 24226387]
41. White RM, Sessa A, Burke C, Bowman T, LeBlanc J, Ceol C, Bourque C, Dovey M, Goessling W, Burns CE, Zon LI. Transparent adult zebrafish as a tool for in vivo transplantation analysis. Cell stem cell. 2008; 2:183–189. [PubMed: 18371439]
42. Haldi M, Ton C, Seng WL, McGrath P. Human melanoma cells transplanted into zebrafish proliferate, migrate, produce melanin, form masses and stimulate angiogenesis in zebrafish. Angiogenesis. 2006; 9:139–151. [PubMed: 17051341]
43. Corkery DP, Dellaire G, Berman JN. Leukaemia xenotransplantation in zebrafish--chemotherapy response assay in vivo. British journal of haematology. 2011; 153:786–789. [PubMed: 21517816]

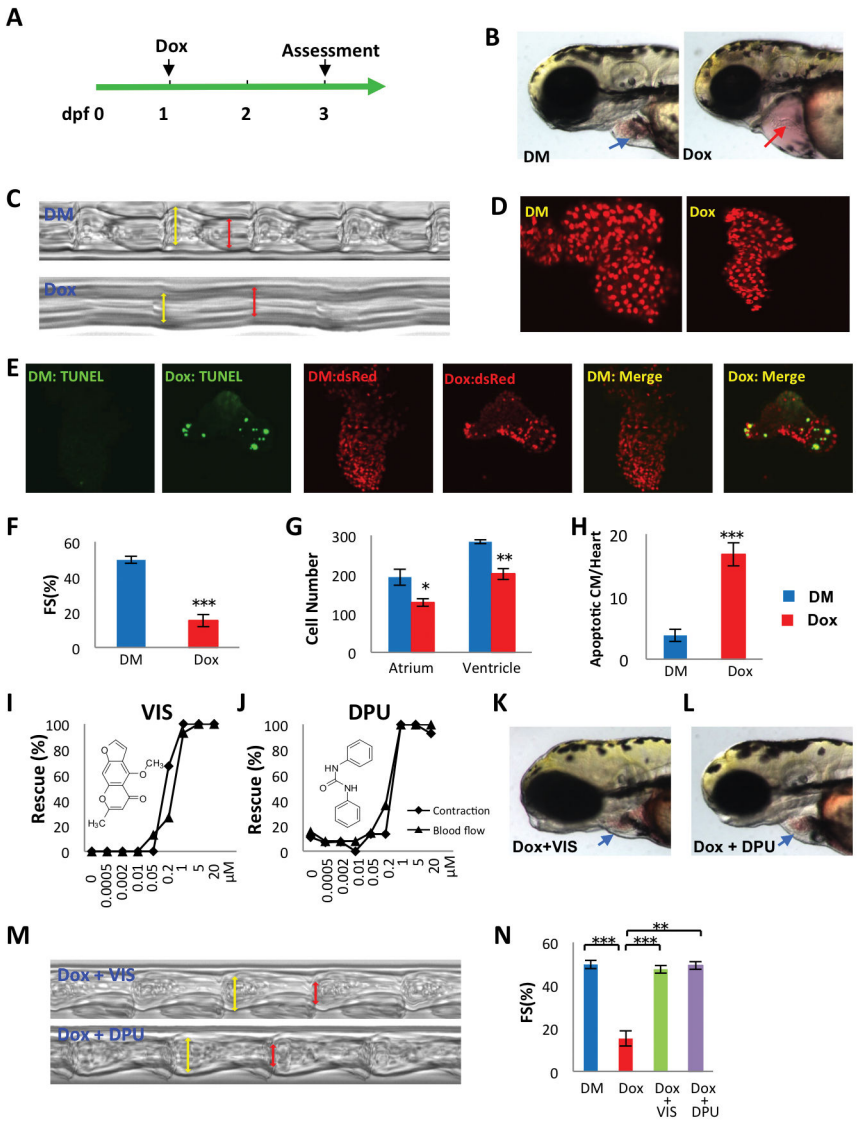


**Fig 1. Discovery of doxorubicin suppressors VIS and DPU in a doxorubicin-induced cardiomyopathy model in zebrafish**

**(A)** Experimental scheme for inducing cardiomyopathy in zebrafish. (dpf, days post fertilization; Dox, doxorubicin) **(B)** Representative images of a normal heart (blue arrow) and doxorubicin-treated heart (red arrow).(DM, DMSO control) **(C, M)** Images reflecting heart contraction over time, derived from a region of interest drawn across the ventricle in sequential frames of high speed video of the beating heart. **(D)** Representative images of cardiomyocytes genetically labeled with nuclear dsRed driven by a cardiomyocyte-specific myl7 promoter. **(E)** Detection of apoptotic cardiomyocyte by TUNEL staining. Green, TUNEL, red, cardiomyocytes, yellow, apoptotic cardiomyocytes. **(F,N)** Quantification of fractional shortening (FS) as follows $(VID_d\text{-}VID_s)/VID_d \times 100$. $VID_d$, diastolic ventricular internal dimension; $VID_s$, systolic ventricular internal dimension. n = 13–19 fish in each group, compared using Student's T-test. **(G)** Quantification of cardiomyocyte number. n = 5 fish in each group, compared using Student's T-test. **(H)** Quantification of apoptotic

cardiomyocytes (CM). n = 5 fish in each group, compared using Student's T-test. **(I,J)** VIS and DPU rescued heart contraction and blood flow in a dose dependent manner, as manifested by the percentage of normal looking fish out of total number of doxorubicin treated fish **(K,L)** Representative images showing grossly normal heart morphology in VIS or DPU rescued zebrafish. DM, DMSO treated control samples; Dox, doxorubicin treated samples; Dox + VIS, doxorubicin and VIS co-treated samples; Dox + DPU, doxorubicin and DPU co-treated samples. Statistics (compared to doxorubicin treated samples): * $p< 0.05$, ** $p<0.01$, and *** $p<0.001$.

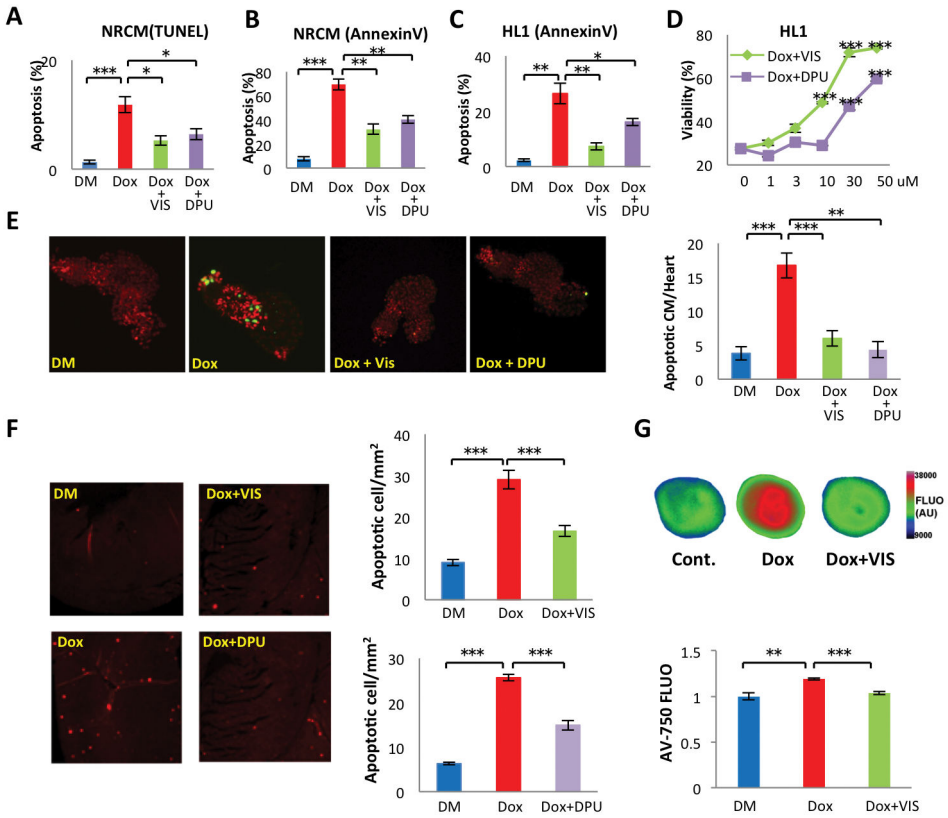


**Fig 2. VIS and DPU effects on doxorubicin-induced cardiac cell death *in vitro* and *in vivo***

Doxorubicin treated neonatal rat cardiomyocytes were treated with VIS and DPU and assessed for apoptosis with TUNEL **(A)** or AnnexinV **(B)** staining. **(C)** Doxorubicin treated HL1 cells were treated with VIS or DPU and assessed for apoptosis with Annexin V staining. **(D)** Viability of HL1 cells treated with doxorubicin and VIS or DPU. Effect of VIS or DPU on cardiac cell death in doxorubicin treated zebrafish **(E)** and mice **(F)** as measured by TUNEL assay. n = 4–5 mice per group. **(G)** Effect of VIS on doxorubicin-induced apoptosis in heart as assessed by *ex vivo* imaging of the whole heart with the dye AnnexinV-750. n = 5 mice per group, compared using one-way ANOVA and the Tukey post-test. DM – DMSO treated control samples, Dox – doxorubicin treated samples, Dox + VIS – doxorubicin and VIS co-treated samples, Dox + DPU – doxorubicin and DPU co-treated samples. Statistics (compared to doxorubicin treated samples): * $p < 0.05$, ** $p<0.01$, and *** $p<0.001$.

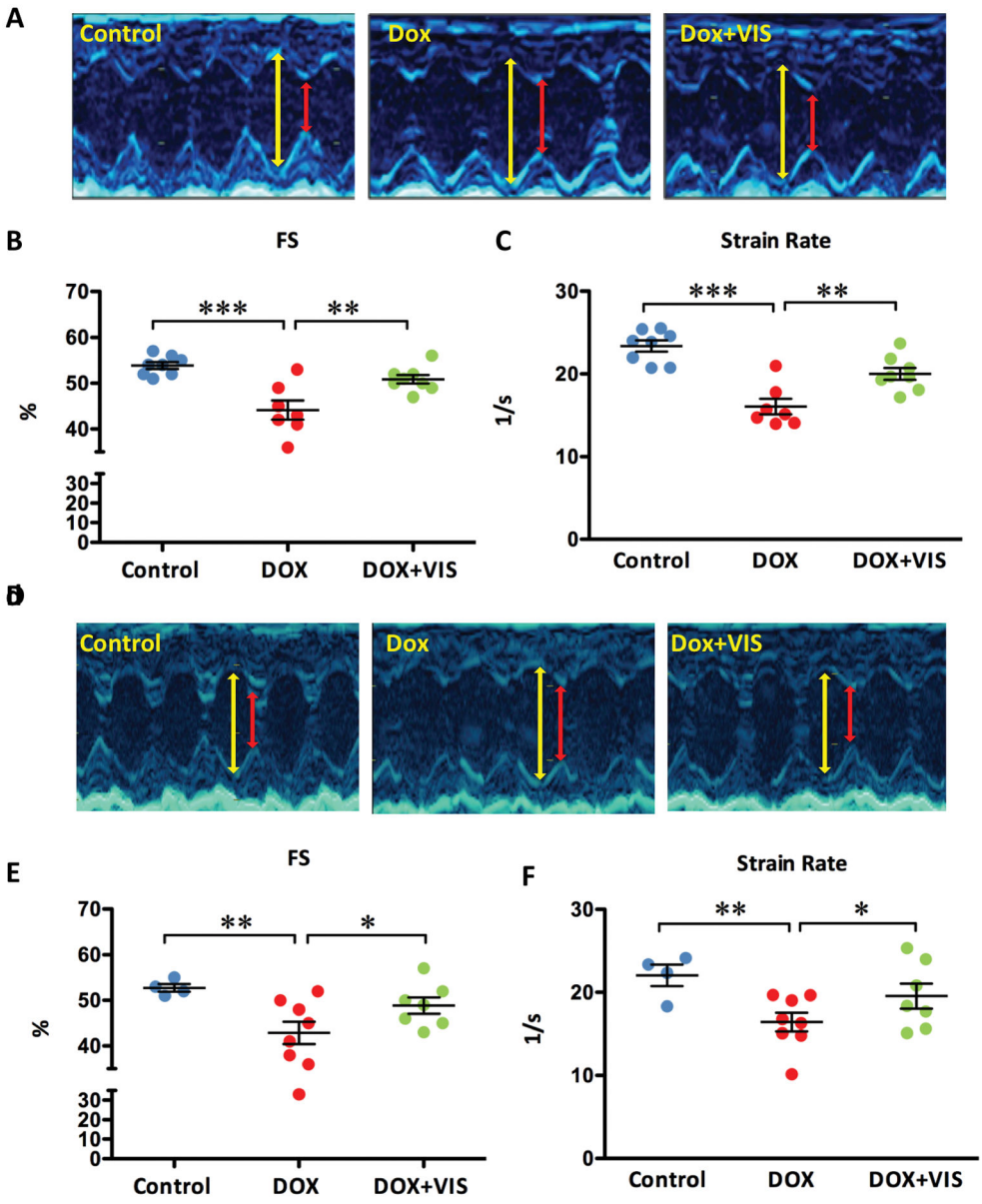


**Fig 3. VIS effect on heart function in doxorubicin treated mice**

Representative M-mode echocardiogram images of acute **(A)** and chronic **(D)** models: yellow line denotes diastolic left ventricle internal dimension (LVIDd) and red line denotes systolic left ventricle internal dimension (LVIDs). Effects of doxorubicin with and without VIS on fractional shortening **(B,E)** and strain rate **(C,F)** in both acute **(B,C)** and chronic **(E,F)** models. For acute models **(B,C)**, groups were compared using one-way ANOVA followed by the Tukey post-test. For chronic models **(E,F)**, groups were compared using one-way ANOVA followed by a one-tailed Student's T-test. Cont – vehicle treated control mice, Dox – doxorubicin treated mice, Dox + VIS – doxorubicin and VIS co-treated mice. Statistics (compared to doxorubicin treated samples): * $p < 0.05$, ** $p<0.01$, and *** $p<0.001$.

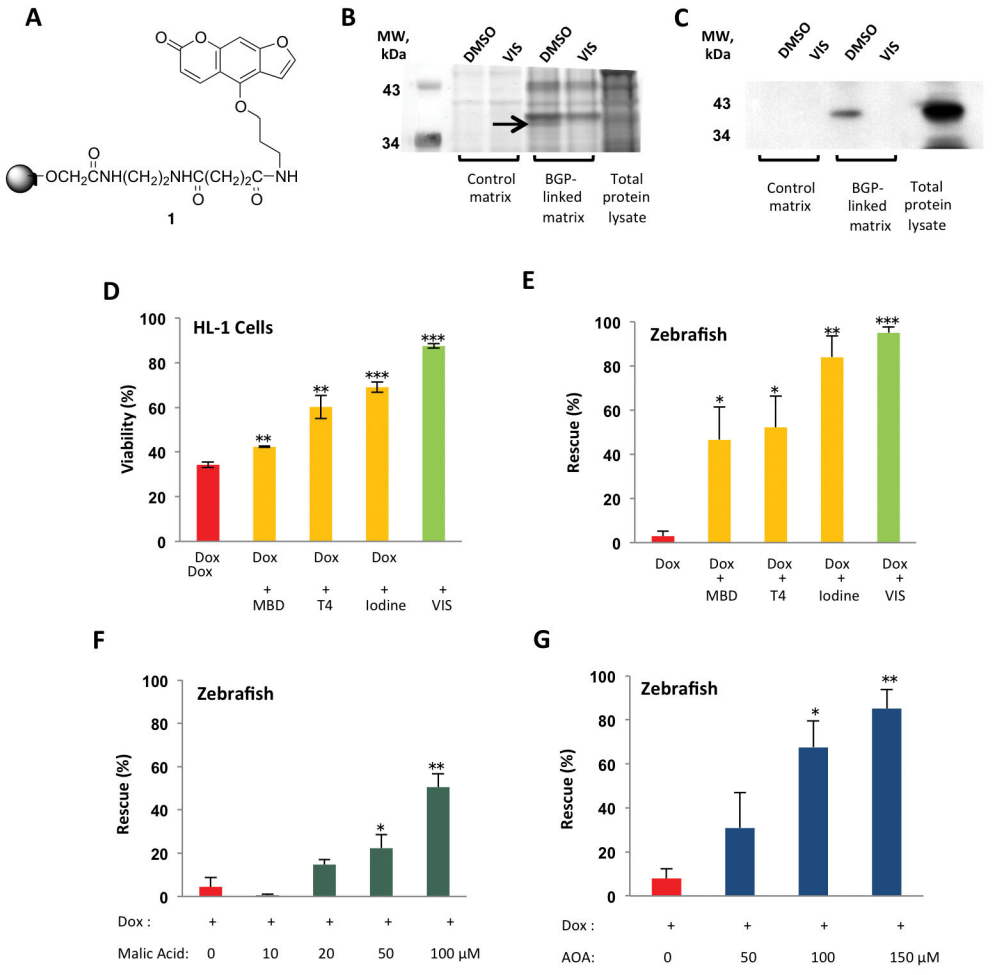


**Fig 4. VIS protects against doxorubicin cardiotoxicity via inhibition of MDH2**

**(A)** Bergapten, a potent VIS derivative, with an alkyl linker that could be attached to a solid support (Compound 1). **(B)** Affinity chromatography using a bergapten-linked matrix and competitive elution with VIS. BGP, bergapten; DM, dimethyl sulfoxide. **(C)** Western blot of gel in (B) incubated with an anti-MDH2 antibody. **(D)** Viability was measured in HL-1 cardiomyocytes treated with doxorubicin and MDH2 inhibitors. **(E)** Rescue from doxorubicin-induced cardiotoxicity and death in zebrafish co-treated with MDH2 inhibitors.. MBD, mebendazole; T4, L-thyroxine. Data were collected over 5 independent experiments, with a total of 150 zebrafish larvae treated for each condition. **(F)** L-malic acid protects against doxorubicin-induced cardiotoxicity and death in a dose-dependent fashion. **(G)** The malate-aspartate shuttle inhibitor AOA protects against doxorubicin-induced cardiotoxicity and death in a dose-dependent fashion. AOA, aminooxyacetate. For panels **(D)-(G)**, data were collected from a total of 150 zebrafish larvae treated for each condition, as measured over 5 independent experiments. % Viability and % Rescue are depicted as mean +/− standard error of the mean. * $p < 0.05$, ** $p<0.01$, and *** $p<0.001$ using a two-tailed Student's T-test.

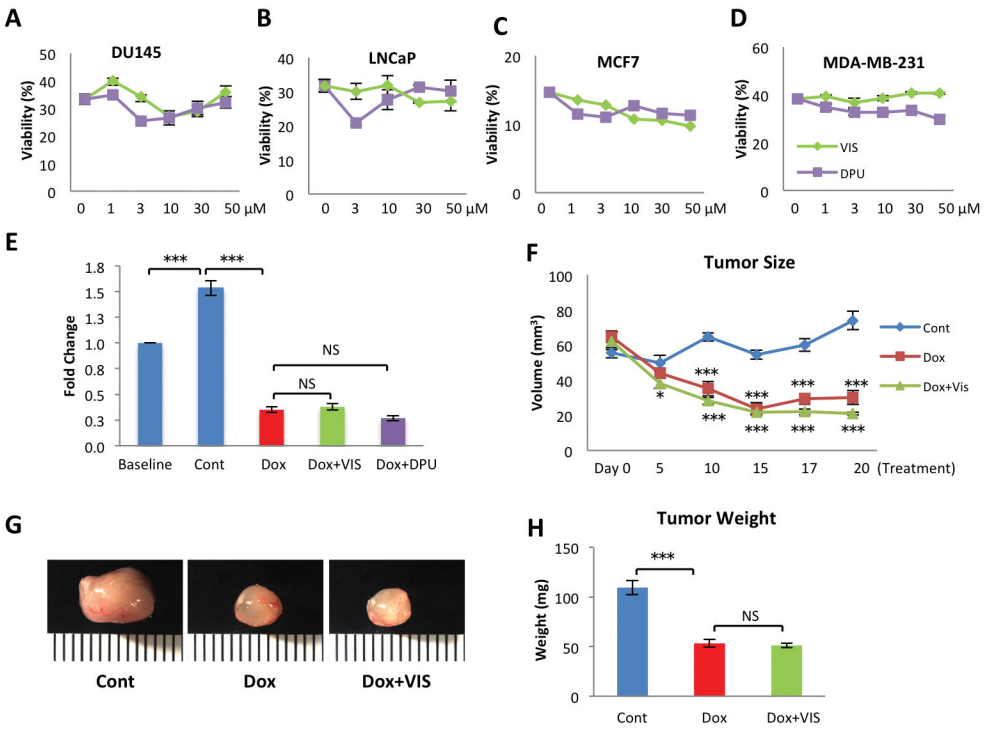


**Fig 5. Lack of protective effect of VIS nor DPU on tumor cells *in vitro* or *in vivo***

Cell viability in multiple tumor lines including DU145 **(A)**, LNCaP **(B)**, MCF7 **(C)** and MDA-MB-231 **(D)** treated with VIS or DPU.. **(E)** Fold change in size of xenografted human tumor derived from Jurkat cell injection in zebrafish *in vivo* treated with either VIS or DPU. **(F)** Tumor volume in human tumor xenograft derived from injected MDA-MB-231 cells in mice treated with doxorubicin and VIS. Tumor size was assessed by caliper measurement of long axis a, short axis b and was calculated with equation $V=1/2*a*b^2$. n = 8 mice in each group. **(G)** Representative images of postmortem tumors from the three groups. **(H)** Effect of VIS on Dox inhibition of tumor growth.Cont – vehicle treated control samples, Dox – doxorubicin treated samples, Dox + VIS – doxorubicin and VIS co-treated samples, Dox + DPU – doxorubicin and DPU co-treated samples. NS, non-significant. Statistics (compared to doxorubicin treated samples): * $p< 0.05$, ** $p<0.01$, and *** $p<0.001$.

**Table 1**

Acute Doxorubicin-induced Cardiomyopathy Mouse Model

| | Control | Dox | Dox + VIS |
|---|---|---|---|
| **HR, beats/min** | 710±15 | 605±23** | 640±17* |
| **LVIDd, mm** | 3.22±0.05 | 3.19±0.09 | 3.08±0.06 |
| **LVIDs, mm** | 1.48±0.04 | 1.78±0.10* | 1.51±0.04‡ |
| **FS, %** | 54±1 | 44±2*** | 51±1‡‡ |
| **Strain Rate, 1/s** | 23±1 | 16±1*** | 20±1*‡‡ |
| **N** | 8 | 7 | 8 |

Values are presented as mean ± SEM;

*$P<0.05$

**$P<0.01$

***$P<0.001$ *vs.* Control;

‡$P<0.05$,

‡‡$P<0.01$, *vs.* Dox.

**Table 2**

Chronic Doxorubicin-induced Cardiomyopathy Mouse Model

| | Control | Dox | Dox+Vis |
|---|---|---|---|
| **HR, beats/min** | 752±14 | 678±14** | 707±21 |
| **LVIDd, mm** | 3.26±0.1 | 3.33±0.04 | 3.42±0.08 |
| **LVIDs, mm** | 1.54±0.07 | 1.91±0.1* | 1.76±0.09 |
| **FS, %** | 53±1 | 43±2** | 49±2‡ |
| **Strain Rate, 1/s** | 22±1 | 16±1** | 20±2‡ |
| **N** | 4 | 8 | 7 |

Values are presented as mean ± SEM;

*$P<0.05$

**$P<0.01$

***$P<0.001$ *vs.* Control;

‡$P<0.05$,

‡‡$P<0.01$, *vs.* Dox.